Optical system design with conformal decentered and tilted elements

Jun Chang (常 军)[1*], Wubin He (何伍斌)[1], Ruirui Wang (王蕊瑞)[1], and Shulong Feng (冯树龙)[2]

[1]*Laboratory of Optoelectronics Technology and Information System, School of Optoelectronics, Beijing Institute of Technology, Beijing 100081, China*

[2]*Changchun Institute of Optics, Fine Mechanics and Physics, Chinese Academy of Sciences, Changchun 343100, China*

[*]*Corresponding author: bitchang@bit.edu.cn*

Received September 7, 2010; accepted November 15, 2010; posted online February 21, 2011

We investigate the aberration properties of the conformal optical system with decentered and tilted elements by vector aberration theory. By decentering and tilting the window and corrector of the system, two elements are effectively used together in a particular manner by aberration compensation to achieve off-axis imaging. A conceptual design is performed with a half-field of 2°, the F# of 4, and the wavelength ranging of 3700−4800 nm. The imaging quality can reach the optical diffraction limit and satisfy corresponding requirements.

OCIS codes: 220.4830, 220.1010.
doi: 10.3788/COL201109.032201.

At present, increasing number optical devices are beginning to adopt decentered and tilted optical system[1−5]. Some of them are based on the consideration of imaging performance, such as non-obscuration with large field optical systems; some are based on the consideration of overall structure, such as in the need to place other non-optical components on the axis of a system (electronic components or mechanical components, etc.); others are applications in special areas, such as projection display systems of perspective helmets[6,7].

A conformal optical system, with its excellent aerodynamic performance, is drawing increasing attention, and will be widely applied to various types of aircraft[8]. A conformal window can be coaxial or off-axis, such as the free form of Airfoil, etc. Multiple institutes have conducted systematic research on coaxial optical systems, including dynamic performance, aberration characteristics[9], and optical correction devices design[10,11]. However, few studies focusing on non-coaxial optical systems have been conducted, and even domestic literature on this point is limited. First, designing decentered and tilted optical systems is difficult, and the aberration theory of current designs for coaxial optical systems cannot be directly applied to decentered and tilted optical systems. Second, the non-central symmetry aberration is rather complicated for conformal windows; thus, the application of off-axis aberration theory in conformal optical systems will be a very significant attempt.

In this letter, we review the vector aberration theory of decentered and tilted optical systems and analyse the aberration characteristics of conformal systems with the decentered windows. According to the aberration characteristics of the conformal system, the spherical aberration, coma, and astigmatism terms in wavefront polynomials are selected. Then, we adopt aberration compensation methods, and make appropriate decentered and tilted adjustments on the optical corrector to eliminate the image effect from the decentered window. Finally, we analyze the spot diagrams and modulation transfer function (MTF) curves through optical design software. Results show that this method can address the challenges in off-axis conformal optical systems.

In a centered, rotational symmetric optical system, the Seidel polynomial of wavefront aberration in vector form is[12]:

$$W = \sum_j W_j = \sum_j W_{040j}(\vec{\rho}\cdot\vec{\rho})^2 + \sum_j W_{131j}(\vec{H}\cdot\vec{\rho})(\vec{\rho}\cdot\vec{\rho}) + \sum_j W_{222j}(\vec{H}\cdot\vec{\rho})^2 + \sum_j W_{220j}(\vec{H}\cdot\vec{H})(\vec{\rho}\cdot\vec{\rho}) + \sum_j W_{311j}(\vec{H}\cdot\vec{H})(\vec{H}\cdot\vec{\rho}), \quad (1)$$

where $\vec{H}$ is the normalized field point height; $\vec{\rho}$ denotes the normalized pupil redius coordinates; W_j represents the optical path difference of actual wavefront

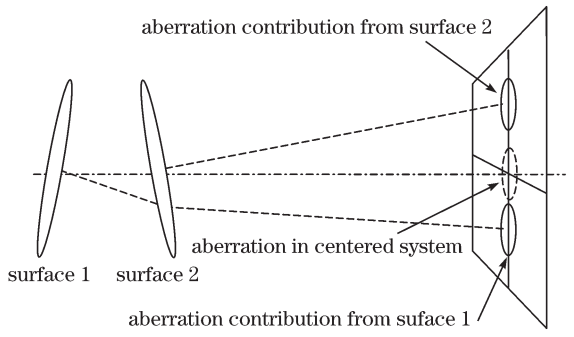

Fig. 1. Decentered and titled aberration contributions from rotationally symmetric subsystems.

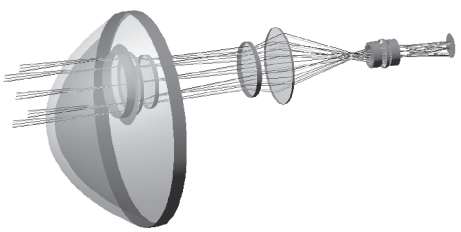

Fig. 2. Decentered window 20 mm.

and reference surface wavefront; W_{040}, W_{131}, W_{222}, W_{220}, and W_{311} represent the third-order spherical aberration, third-order coma, third-order astigmatism, third-order field curvature, and third-order distortion coefficients, respectively.

In a decentered and tilted optical system, wavefront coefficients will change, but two points are worth paying special attention to[13]: 1) the image plane aberration field is still the total number of contributions from each surface aberration; 2) in a system of tilted spherical components, the symmetry axes for the aberration contributing subsystems are not mutually aligned, and their aberration contributions therefore appear at different points in the image field, as indicated conceptually in Fig. 1[14]; $\vec{\sigma}_j$ is the decenter of the center of aberration field W_j with respect to the unperturbed field center. Thus, after joining the decentered and tilted systems, the wavefront aberration expanded function is[15]:

$$W = \sum_j W_{040j}(\vec{\rho}\cdot\vec{\rho})^2 + \sum_j W_{131j}[(\vec{H}-\vec{\sigma}_j)\cdot\vec{\rho}](\vec{\rho}\cdot\vec{\rho}) + \sum_j W_{222j}[(\vec{H}-\vec{\sigma}_j)\cdot\vec{\rho}]^2 + \sum_j W_{220j}[(\vec{H}-\vec{\sigma}_j)\cdot(\vec{H}-\vec{\sigma}_j)](\vec{\rho}\cdot\vec{\rho}) + \sum_j W_{311j}[(\vec{H}-\vec{\sigma}_j)\cdot(\vec{H}-\vec{\sigma}_j)][(\vec{H}-\vec{\sigma}_j)\cdot\vec{\rho}]. \quad (2)$$

It is similar to coaxial wavefront polynomial function; after the introduction of tilts or decentrations, spherical aberration, comas, and astigmatism are still the top three elements of wavefront aberration function; that is, the first, second, and third terms in the Eq. (2). From Eq. (2) we can see that the first term is unaffected by tilts or decentrations. The other two terms contain $\vec{\sigma}_j$; thus, the third-order coma and third-order astigmatism are

$$W_{\text{coma}} = W_{131}(\vec{H}\cdot\vec{\rho})(\vec{\rho}\cdot\vec{\rho}) - (\vec{A}_{131}\cdot\vec{\rho})(\vec{\rho}\cdot\vec{\rho}), \quad (3)$$

$$W_{\text{asti}} = W_{222}(\vec{H}\cdot\vec{\rho})^2 - (\vec{A}_{222}\cdot\vec{\rho})(\vec{H}\cdot\vec{\rho}) + \sum_j W_{222j}(\vec{\sigma}_j\cdot\vec{\rho})^2, \quad (4)$$

where

$$W_{131} = \sum_j W_{131j}, \quad \vec{A}_{131} = \sum_j W_{131j}\cdot\vec{\sigma}_j,$$
$$W_{222} = \sum_j W_{222j}, \quad \vec{A}_{222} = 2\sum_j W_{222j}\cdot\vec{\sigma}_j.$$

For convenient analysis, the abovementioned equations can be normalized as

$$W_{\text{coma}} = W_{131}[(\vec{H}-\vec{a}_{131})\cdot\vec{\rho}](\vec{\rho}\cdot\vec{\rho}), \quad (5)$$

$$W_{\text{asti}} = W_{222}[(\vec{H}-\vec{a}_{222})^2 + \bar{b}_{222}^2](\vec{\rho}\cdot\vec{\rho}), \quad (6)$$

where

$$\vec{a}_{131} = \vec{A}_{131}/W_{131}, \quad \bar{a}_{222} = \overline{A}_{222}/W_{222},$$
$$\bar{b}_{222}^2 = \overline{B}_{222}^2/W_{222} - \bar{a}_{222}^2.$$

From Eqs. (5) and (6), we can see that coma zero point coordinates are determined by vector $\vec{a}_{131}$, and astigmatism zero point coordinates are determined by vector $\bar{a}_{222} \pm \mathrm{i}\bar{b}_{222}$.

If surface tilt angle is

$$\beta_{0i} = \beta_i + c_i\delta v_i = c_i\delta c_i, \quad (7)$$

where β_i is the tilt about the surface vertex, c_i is the curvature, and δc_i is the decenter.

The image field displacement normalized to the paraxial image height $\bar{y}$ can be changed into

$$\delta q_i' = \delta q_i + y_i\Delta(n_i)\beta_{0i}/L, \quad (8)$$

where y and $\overline{y}$ are the paraxial marginal and chief ray heights at the surface, respectively, $\Delta(n)$ is the change in refractive index at the surface, and L is the Lagrange invariant.

The purpose of discussions on vector aberration theory is to provide the aberration characteristics and variation principles in decentered and tilted optical systems, derive the law of aberration compensation from it, and then create optical system designs.

The idea of this paper is to make the decentered and tilted adjustments on conformal optical system components, and then analyze the changes in aberrations; finally, through the aberration compensation we can obtain the designs of conformal systems with decentered windows.

On the basis of the coaxial system, we decentered the window vertically downward ($-y$ axis). From the optical simulation after the system window decentered, we can see that the aberration of the image plane downward shifts and tilts. In accordance with the idea of aberration compensation, and without changing the group of imaging lenses, the optical corrector will have appropriate tilt, making its aberration field reverse tilt and upward shift. Image field displacement $\delta q_i'$ under the two changes can be offset to ensure the field center of image at the origin position. Figures 2 and 3 show the layout of the decentered window and tilted optical corrector. Then, we need to make detailed analysis on aberrations, and find the coma and astigmatism zero position, that is, $\vec{a}_{131}$ and $\vec{a}_{222} \pm i\bar{b}_{222}$, and then obtain appropriate compensation programs. Figure 4 shows the spot diagram and astigmatism distributed map of the conformal system with the decentered window; figure 5 shows the spot diagram and astigmatism distributed map of the conformal system with the tilted optical corrector.

From Fig. 4, we can see that image plane, tilt defocus and coma are introduced after the window verticuly down warding at 20 nm. Using Zernike polynomi-

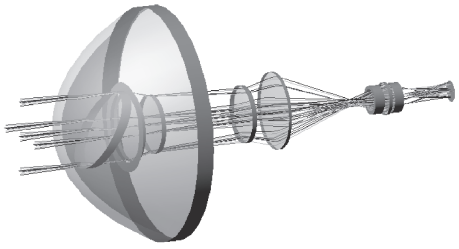

Fig. 3. Tilted optical corrector 20°.

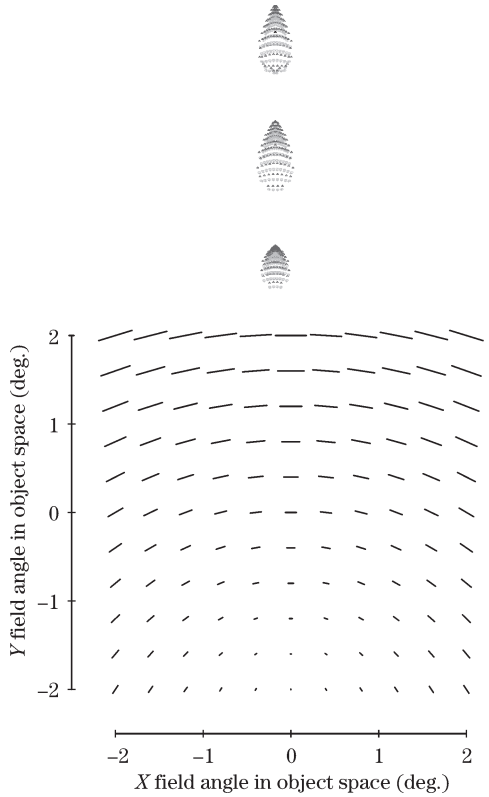

Fig. 4. Spot diagram and astigmatism distributed map of conformal system with decentered window.

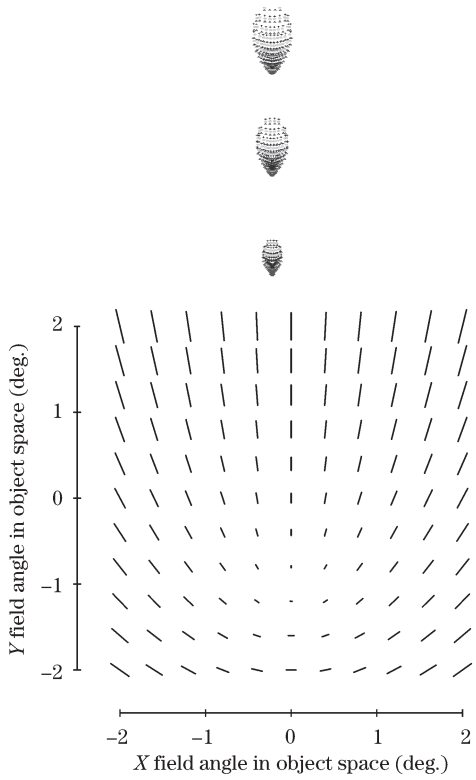

Fig. 5. Spot diagram and astigmatism distributed map of conformal system with tilted optical corrector.

als, we fit the system exit pupil and obtain a tilted angle of about $-3.72°$. The field center of the image moves vertically downward ($-y$ axis) to 2.91 mm. From the spot diagrams and the ray aberration curves, we can see that the change in coma is larger than those in others and it turns from coaxial 1.6 to 20 μm, and relative to the x-axis direction of $-90°$. From the third-order astigmatism distribution map, we can see that the astigmatism direction is consistent with the $-y$ axis, and the value of astigmatism under full-aperture and full-field is changes from -9.344 to -158 μm.

From Fig. 5, we can see that after the corrector tilting at 20°, image plane tilt, astigmatism, and coma are introduced. The image surface tilts by 2.31° and the field. center of the image moves vertically upward ($+y$ axis) to 2.62 mm. From the spot diagrams and ray aberration curves, we know that the coma turns from 1.6 to 28 μm, and relative to the x axis direction of 90°. From the third-order astigmatism distribution map, the astigmatism direction is consistent with the y axis; the value of astigmatism under full-aperture and full-field changes from -9.344 to 148 μm.

From the analysis above, we can determine the opposite trend of aberration in two cases, which can be used for aberration compensation. We combine the decentered window with the tilted optical corrector and then obtain the final design results, as shown in Fig. 6. The system parameters are: $F\#$ is 4, the half-field angle is 2°, the incident wavelengths range from 3700 to 4800 nm, pupil diameter is 30 mm, and focal length is 120 mm. The thicknesses of the window and optical corrector are 4 and 4.7 mm, respectively. The window is decentered vertically downward ($-y$ axis) to 20 mm, the optical corrector tilts in a clockwise direction relative to the vertical

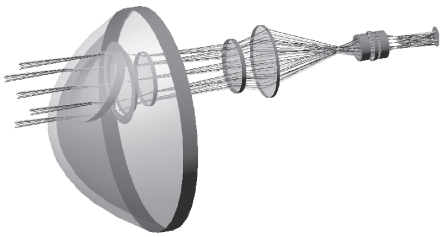

Fig. 6. Layout of systematic structures.

26°, the parameters of the subsequent imaging lenses are unchanged and are identical to the coaxial system. The lens data of the system is shown in Table 1.

According to the vector aberration theory mentioned above, when the window is decentered and the corrector tilted, the image field will also be tilted. However, in the two cases, the tilt directions are opposite; according to Eq. (7), we identify a direction where the zero point is vertical to the optical axis. At the same time, field center and aberration are displaced from the vertical optical axis. The deviation vectors are $\vec{\sigma}_1$ and $\vec{\sigma}_2$, and they are in the opposite direction.

Both the tilted optical corrector and decentered window change the location of the zero point in the image field, but if we choose a specific relationship (in this design, the decentered value is -20 mm, according to aberration compensation, the tilt angle we chose is 26°), the zero point of the coma and symmetry center of two astigmatism points can be located in the center of the image field. As the coaxial system aberrations are poised, spherical aberration, coma, and field curvature are corrected. Thus, the symmetry center of two astigmatism

Table 1. Lens Data of the System

Surface	Surface Type	Radius	Thickness	Glass	Semi-Aperture	Non-Centered Data
Object	Sphere	Infinity	Infinity			
1	Conic	35.222	4.000	MGF_2E	50.000	Decenter & Return
2	Conic	32.085	11.971		49.000	Decenter & Return
3	Zernike Polynomial	Infinity	4.701	MGF_2E	15.038	Decenter & Return
4	Zernike Polynomial	Infinity	5.163		14.865	Decenter & Return
Stop	Sphere	Infinity	0.100		16.180	Decenter &
Image	Sphere	Infinity	−5.529		4.500	Return

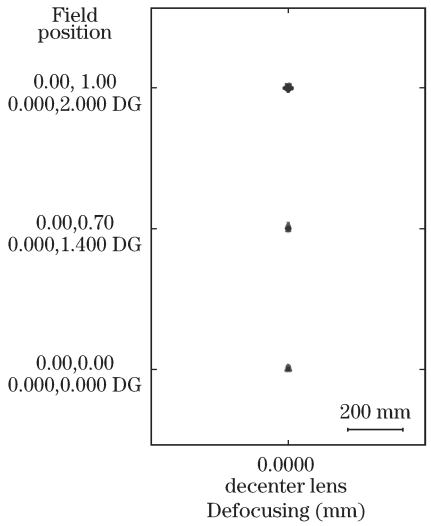

Fig. 7. Spot diagram.

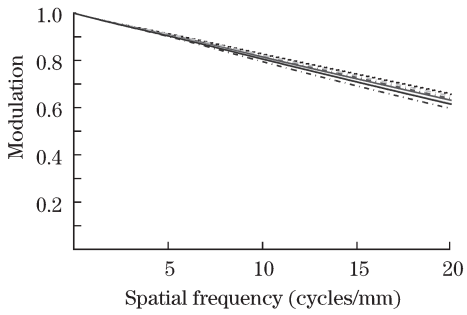

Fig. 8. MTF plot.

points can be located in the center of the image field. $W_{222} = 0$, $W_{131} = 0$, and $W_{220} = 0$; the two vectors have different values and opposite directions. Then, according to Eq. (5), the coma in the entire field should be zero, and according to Eq. (6), the astigmatism in the entire field should be constant in value and unchanging in direction. From the system simulation results by the optical software, we can see that the coma is reduced to 5 μm and the value of astigmatism under full-aperture and full-field is reduced to 15 μm.

Figure 7 is the spot diagram; the root mean square spot diameter of the entire field is 13 μm. Figure 8 is the system transfer function curve, it reaches 0.615 (diffraction limit is 0.632) at 20 Lp/mm. From the map, we can see that image quality is approaching the diffraction limit, and the exit pupil distance and exit pupil diameter satisfy infrared system requirements.

Finally, the 20-mm window decentration is intended to show the feasibility of conformal systems with large decentrations and tilt components. In fact, taking optical-mechanical assembly and engineering application into consideration, the decentration can be appropriately increased to 30 mm. Furthermore, this particular design method of infrared IR-system can be extended to the visible-light optical system.

In conclusion, vector aberration theory is introduced to conformal optical systems. The aberration characteristics of components with large decentrations and tilts is studied. We combine two components in a particular way according to aberration compensation, and the final design results achieve the purpose of off-axis imaging. The results can serve as reference to solve similar problems.

References

1. X. Yang, Z. Wang, G. Mu, and R. Fu, Photo. Technol. Journal (in Chinese) **34,** 1658 (2005).
2. L. Fang, X. He, Y. Wang, and Y. Gong, Acta Opt. Sin. (in Chinese) **6,** 45 (2010).
3. Y. Feng, X. Wang, H. Yang, and C. Zhou, Chinese J. Lasers (in Chinese) **37,** 1734 (2010).
4. J. Chang, M. Zou, R. Wang, S. Feng, and M. M. Talha, Chin. Opt. Lett. **8,** 1082 (2010).
5. G. Lai, G. Shen, and R. Geisler, Chin. Opt. Lett. **7,** 1126 (2009).
6. X. Fan, R. Chen, Z. Ma, and Y. Ma, Photon. Science (in Chinese) **33,** 494 (2004).
7. J. Tong, Q. Cui, C. Xue, C. Pan, D. Zhang, and K. Zhang, Acta Opt. Sin. (in Chinese) **30,** 2662 (2010).
8. P. A. Trotta, Proc. SPIE **4375,** 96 (2001).
9. B. G. Crowther, D. B. McKenney, and J. P. Mills, Proc. SPIE **3482,** 48 (1998).
10. T. A. Mitchell and J. M. Sasian, Proc. SPIE **3705,** 209 (1999).
11. D. J. Knapp, Proc. SPIE **4832,** 394 (2002).
12. K. Thompson, "Aberration fields in tilted and decentered optical systems", PhD. Thesis (University of Arizona, 1980).
13. J. R. Rogers, Proc. SPIE **3737,** 286 (1999).
14. T. S. Turner, Jr., Proc. SPIE **1752,** 184 (1992).
15. J. R. Rogers, Opt. Eng. **139,** 776 (2000).